Free Energy from Stationary Implementation of the DFT + DMFT Functional

Kristjan Haule and Turan Birol

Department of Physics and Astronomy, Rutgers University, Piscataway, New Jersey, USA
(Received 27 January 2015; published 16 December 2015)

The stationary functional of the density functional plus embedded dynamical mean field theory formalism to perform free energy calculations and structural relaxations is implemented for the first time. Here, the first order error in the density leads to a much smaller, second order error in the free energy. The method is applied to several well-known correlated materials: metallic $SrVO_3$, Mott insulating FeO, and elemental cerium, to show that it predicts the lattice constants with good accuracy. In cerium, we show that our method predicts the isostructural transition between the α and γ phases, and resolve the long-standing controversy in the driving mechanism of this transition.

Prediction of the crystal structures of solids by large scale quantum mechanical simulations is one of the fundamental problems of condensed matter physics, and occupies a central place in materials design. The workhorse of the field is the density functional theory (DFT) [1] at the level of local density approximation (LDA) or generalized gradient approximations (GGAs), which predict lattice constants of weakly correlated materials typically within ~1% relative error [2].

These errors of DFT in LDA or GGA implementations are an order of magnitude larger in the so-called correlated materials: For example, the lattice constant of δ-Pu is underestimated by 11% [3] or nonmagnetic FeO by 7% [4]. While GGAs and hybrid functionals can sometimes improve upon conventional LDA, these functionals many times degrade the agreement between predicted and experimentally determined bulk moduli and lattice constants, in particular in materials containing heavy elements [2].

To account for the correlation effects, more sophisticated many body methods have been developed. Among them, one of the most successful algorithms is the dynamical mean-field theory (DMFT) [13]. It replaces the problem of describing correlation effects in a periodic lattice by a strongly interacting impurity coupled to a self-consistent bath [14]. To become material specific, DMFT was soon developed into an electronic structure tool (DFT + DMFT) [15,16], which achieved great success in numerous correlated materials (for a review see Ref. [17]). The DFT + DMFT method has mainly been used for the calculation of spectroscopic quantities, and only a few dozen [18–38] of studies managed to compute energetics of correlated solids, and only a handful of them used exact solvers and charge self-consistency [26,27,32,33,36,37]. This is not only because of the very high computational cost, but also because previous implementations of DFT + DMFT were not stationary, and hence it was hard to achieve the precision of free energies needed for structure optimization and the study of phase transitions in solids.

Here we implemented the DFT + DMFT functional in the real space embedded DMFT approach [39], which delivers stationary free energies at finite temperatures. This stationarity is crucial for practical implementation and precision of computed energies, since the first order error in the density ρ (or the Green's function) leads only to the much smaller second order error in the free energy, since the first order variation vanishes, i.e., $\delta F / \delta \rho = 0$. This property is also crucial in calculating the forces, as stationarity of the functional ensures that only Hellmann-Feynman forces need to be computed for structural relaxation [40].

The DFT + DMFT total energy is given by [17]

$$E = \mathrm{Tr}(H_0 G) + \frac{1}{2}\mathrm{Tr}(\Sigma G) + E^H[\rho] + E^{xc}[\rho]$$
$$- \Phi^{\mathrm{DC}}[n_{\mathrm{loc}}] + E_{\mathrm{nuc\text{-}nuc}} \qquad (1)$$

where $H_0 = -\nabla^2 + \delta(\mathbf{r} - \mathbf{r}')V_{\mathrm{ext}}(\mathbf{r})$, G is the electron Green's function, $E^H[\rho]$ and $E^{xc}[\rho]$ are Hartree and DFT exchange correlation functionals, V_{ext} is the electron-nuclear potential, $E_{\mathrm{nuc\text{-}nuc}}$ is the interaction energy of nuclei, Σ is the DMFT self-energy, and $\Phi^{\mathrm{DC}}[n_{\mathrm{loc}}]$ is the double-counting (DC) functional. [4] Here the Migdal-Galitskii formula (MGF) is used $E_{\mathrm{pot}} = \frac{1}{2}\mathrm{Tr}(\Sigma G)$ to compute the DMFT part of the potential energy.

Gordon Baym showed [41] that for a certain class of approximations, which are derivable from a functional expressed in terms of closed-loop Feynman diagrams, the MGF can be used instead of a more complicated expression for evaluating the Luttinger-Ward Functional [42,43]. He called such approximations conserving. While the DMFT is a conserving approximation in Baym's sense, LDA or GGA is not, as the Galitskii-Migdal formula $\frac{1}{2}\mathrm{Tr}(V_{xc}\rho)$ has to be replaced by the exchange-correlation functional $E^{xc}[\rho]$. As a result, the combination of DFT + DMFT in its charge self-consistent version is not conserving either, and consequently the MGF can give a different

total energy than the Luttinger-Ward functional. Only the evaluation of the latter is guaranteed to give stationary free energies. We will give numerical evidence that evaluation of the MGF in Eq. (1) gives different results than evaluation of the Luttinger-Ward functional, which strongly suggests that Eq. (1) gives nonstationary total energies.

The Luttinger-Ward functional of DFT + DMFT has been well known for several years [17], but it has never been successfully implemented to compute the free energy of solids. It has the following form:

$$\Gamma[G] = \mathrm{Tr} \log G - \mathrm{Tr}[(G_0^{-1} - G^{-1})G] + E^H[\rho]$$
$$+ E^{xc}[\rho] + \Phi^{\mathrm{DMFT}}[\hat{P}G] - \Phi^{\mathrm{DC}}[\hat{P}\rho] + E_{\mathrm{nuc\text{-}nuc}}, \quad (2)$$

where $G_0^{-1}(\mathbf{rr'};i\omega) = [i\omega + \mu + \nabla^2 - V_{\mathrm{ext}}(\mathbf{r})]\delta(\mathbf{r-r'})$, $\Phi^{\mathrm{DMFT}}[\hat{P}G]$ is the DMFT functional, which is the sum of all local skeleton Feynman diagrams. The projected Green's function $\hat{P}G \equiv G_{\mathrm{local}} = \sum_{LL'} |\phi_L\rangle\langle\phi_L|G|\phi_{L'}\rangle\langle\phi_{L'}|$ and the projected density $\hat{P}\rho \equiv \rho_{\mathrm{local}}$ are computed with projection to a set of localized functions $|\phi\rangle$ centered on the "correlated" atom. The projection defines the local Green's function G_{local}, the essential variable of the DMFT.

The variation of functional $\Gamma[G]$ with respect to G ($\delta\Gamma[G]/\delta G$) gives

$$G^{-1} - G_0^{-1} + (V_H + V_{xc})\delta(\mathbf{r-r'})\delta(\tau-\tau')$$
$$+ \hat{P}\frac{\delta\Phi^{\mathrm{DMFT}}[G_{\mathrm{local}}]}{\delta G_{\mathrm{local}}} - \hat{P}\frac{\delta\Phi^{\mathrm{DC}}[\rho_{\mathrm{local}}]}{\delta\rho_{\mathrm{local}}}\delta(\mathbf{r-r'})\delta(\tau-\tau') = 0, \quad (3)$$

which vanishes, since it is equal to the Dyson equation that determines a self-consistent G; hence, the functional is stationary.

The value of the functional Γ at the self-consistently determined G delivers the free energy of the system [41]. We evaluate it by inserting $G_0^{-1} - G^{-1}$ from Eq. (3) into Eq. (2) to obtain

$$F = E_{\mathrm{nuc\text{-}nuc}} - \mathrm{Tr}[(V_H + V_{xc})\rho] + E^H[\rho] + E^{xc}[\rho]$$
$$+ \mathrm{Tr}\log G - \mathrm{Tr}\log G_{\mathrm{loc}} + F_{\mathrm{imp}}$$
$$+ \mathrm{Tr}(V_{dc}\rho_{\mathrm{loc}}) - \Phi^{\mathrm{DC}}[\rho_{\mathrm{loc}}] + \mu N, \quad (4)$$

where we denoted $V_{dc} \equiv \delta\Phi^{\mathrm{DC}}[\rho_{\mathrm{local}}]/\delta\rho_{\mathrm{local}}$ and F_{imp} is the free energy of the impurity problem, i.e., $F_{\mathrm{imp}} = \mathrm{Tr}\log G_{\mathrm{loc}} - \mathrm{Tr}(\Sigma G_{\mathrm{loc}}) + \Phi^{\mathrm{DMFT}}[G_{\mathrm{loc}}]$ [4]. Here we also use the fact that the solution of the auxiliary impurity problem delivers the exact local Green's function, i.e., $\Sigma = \delta\Phi^{\mathrm{DMFT}}[G_{\mathrm{local}}]/\delta G_{\mathrm{local}}$, and we added μN because we work at a constant electron number.

The crucial point is that the continuous time quantum Monte Carlo (CTQMC) method [44,45] solves the quantum impurity model (QIM) numerically exactly; hence, we

can compute very precisely the impurity internal energy as well as the free energy F_{imp} of this model. As the impurity configurations are visited with probability proportional to their contribution to the partition function ($P_k = Z_k/Z$), and since probability for kth order term P_k is easily sampled by CTQMC algorithm, we can compute the value of the partition function Z if we know the partition function at any order of the perturbation theory k. The zeroth order corresponds to the atomic state, hence, $Z_0 = Z_{\mathrm{atom}}$, which can be directly computed from the knowledge of the atomic energies. Hence as long as the probability for zeroth perturbation order is above the QMC noise level ($\approx 10^{-5}$), which is always the case at sufficiently high temperature, we can compute the impurity free energy from

$$F_{\mathrm{imp}} = -T[\log(Z_{\mathrm{atom}}) - \log(P_0)]. \quad (5)$$

This is because $Z = \exp(-F_{\mathrm{imp}}/T)$.

When the temperature is low, P_0 becomes exponentially small, and we can no longer determine F_{imp} to high enough precision in this way. However, we can compute very precisely the internal energy of the impurity at arbitrary temperature. The internal energy of QIM E_{imp} is given by

$$E_{\mathrm{imp}} = \mathrm{Tr}\left[\left(\Delta + \varepsilon_{\mathrm{imp}} - \omega_n \frac{d\Delta}{d\omega_n}\right)G_{\mathrm{imp}}\right] + E_{\mathrm{imp\text{-}pot}}, \quad (6)$$

which follows directly from the thermodynamic average of the QIM Hamiltonian. Here the hybridization Δ and impurity levels $\varepsilon_{\mathrm{imp}}$ are determined from the local green's function by the standard DMFT self-consistency condition $G_{\mathrm{local}}^{-1} = i\omega_n - \varepsilon_{\mathrm{imp}} - \Sigma - \Delta$. These quantities can be computed very precisely by CTQMC calculations [4]; hence, the impurity internal energy can be easily computed with the precision of a fraction of a meV.

To compute the precise impurity free energy F_{imp} at temperature T we first converge DFT + DMFT equations to high accuracy at this temperature T. Using converged impurity hybridization $\Delta(i\omega_n)$ at T, we raise the temperature of the impurity (keeping Δ fixed) to $T_>$, which is chosen such that P_0 becomes of the order of 10^{-5} or higher. This allows us to compute $F_{\mathrm{imp}}(T_>)$ using Eq. (5). We can also compute entropy at $T_>$ from $S_> = [E_{\mathrm{imp}}(T_>) - F_{\mathrm{imp}}(T_>)]/T_>$. Next, we evaluate the impurity internal energy for several inverse temperatures $\beta = 1/T$ between $1/T$ and $1/T_>$, and then we use standard thermodynamic relations to obtain entropy at lower temperature T by

$$S(T) = S_> - \frac{E_{\mathrm{imp}}(T_>)}{T_>} + \frac{E_{\mathrm{imp}}(T)}{T} - \int_{1/T_>}^{1/T} E_{\mathrm{imp}}(1/\beta)d\beta \quad (7)$$

where $\beta = 1/T$. This formula is obtained integrating by parts the standard formula $S = \int c_v/T\, dT$ and $c_v = dE/dT$. We hence obtain S_{imp} and $F_{\mathrm{imp}} = E_{\mathrm{imp}} - TS_{\mathrm{imp}}$ at T which

can be inserted into Eq. (4). The rest of the terms in Eq. (4) are relatively straightforward to evaluate; however, for a high precision implementation one needs to combine the terms that largely cancel and evaluate them together [4].

Previous implementations of free energy within DFT + DMFT [33,35,46] were based on (i) evaluating the total energy Eq. (1) at a range of temperatures, and integrating the resulting specific heat [46], and (ii) the coupling constant integration [33,35], where the total energy of the solid is needed for a range of the Coulomb repulsion's U and is then integrated over U. In both approaches, the self-consistent DFT + DMFT solution is needed for many values of the parameters (either U or T) to evaluate F. In our method, a single DFT + DMFT calculation for a solid is needed, which makes the method much more efficient. Furthermore, current implementation of the free energy is stationary; hence, higher precision of F is achieved.

To test the implementation of the DFT + DMFT functional, we computed the volume dependence of the free energy for three well studied correlated materials: a metallic early transition metal oxide with perovskite structure $SrVO_3$, a Mott insulating transition metal oxide FeO in its rock salt structure, and the lanthanide elemental metal, cerium, in its face centered cubic structure, which undergoes a first order isostructural transition.

We used the implementation of DFT + DMFT of Ref. [39] using the projector or embedding technique, which is based on the Wien2K package[47], and LDA in combination with nominal double counting [39,48,49]. More technical details are given in the Supplemental Material [4].

In Fig. 1(a) we show the energy $E(V)$, and $F(V)$ for $SrVO_3$ at $T = 230$ K, computed with Eq. (1), and Eq. (4), respectively. The minima of $E(V)$ and $F(E)$ are achieved at 55.71 Å^3 and 55.51 Å^3. The experimentally determined volume is $V_{exp} = 56.53$ Å^3 [51]. The DFT + DMFT hence slightly underestimates the equilibrium volume (1.8%), which gives 0.6% error in lattice constant. This is well within the standard error of best DFT functionals for weakly correlated materials.

The metallic nature of $SrVO_3$, with moderate mass enhancements $m^*/m_{band} \approx 2$ [4], leads to very small DMFT corrections in crystal structure [4]. Note that energy minimization leads to slightly larger volume than free energy minimization, contrary to expectations. This is because energy is computed from nonstationary Eq. (1), while free-energy is obtained from the stationary expression Eq. (4). The latter is hence more trustworthy, and should be considered the best DFT + DMFT result. This is also clear from the pressure vs volume diagram in Fig. 1(b), where $-dF/dV$ agrees more favorably with the experiment than $-dE/dV$ obtained by the MGF.

In Fig. 1(c), we show the impurity entropy obtained by Eq. (7) for two representative volumes. In this itinerant system with very large hybridization, we do not notice a temperature scale at which the $t2g$ shell is degenerate
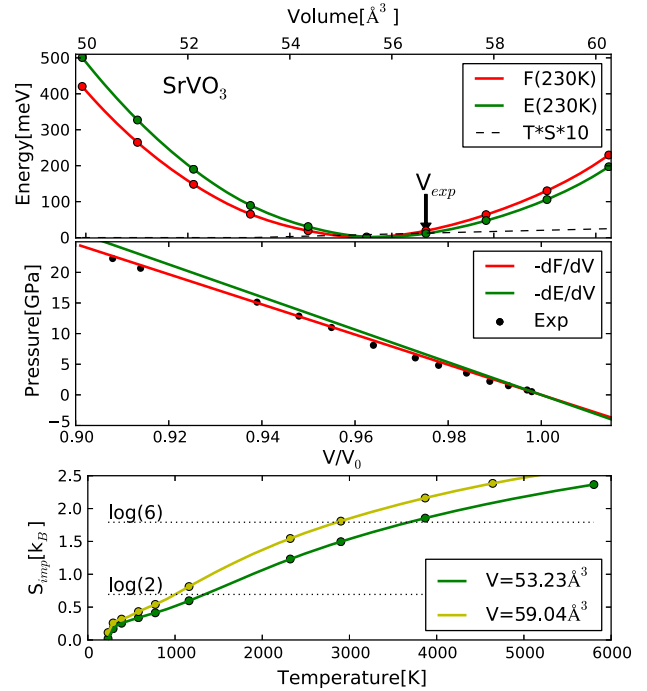

FIG. 1 (color online). (a) $E(V)$ and $F(V)$ for $SrVO_3$ at $T = 230$ K from Eqs. (1) and (4), respectively. Entropy term $TS_{imp}(V)$ is very small. (b) Theoretical and experimental [50] $p(V)$. Good agreement between theoretical $-dF/dV$ and experiment is found. (c) Impurity entropy Eq. (7) for representative volumes. To obtain S_{imp}, temperature is varied in the impurity problem only, and not in the DFT + DMFT problem of the solid.

[log(6)] nor the scale of the lowest order Kramers doublet [log(2)], but we notice the Fermi liquid scale in the steep downturn of $S(T)$ at $T \approx 350$ K.

Figure 2(a) shows $E(V)$ and $F(V)$ for paramagnetic Mott insulating FeO at 300 K, above its antiferromagnetic ordering temperature. The equilibrium volume of E and F is 20.28 Å^3 and 20.24 Å^3, while the experimental volume is 20.342 Å^3. The lattice constant is thus underestimated for only 0.10% and 0.16%, respectively. In comparison, all standard DFT functionals severely underestimate the FeO lattice constant, for example PBE-sol, PBE, and LDA for 5.2%, 5.0%, and 7.7%, respectively.

In Fig. 2(b) we show the $P(V)$ diagram and its excellent agreement with experiment. Figure 2(c) shows impurity entropy $S_{imp}(T)$ for a few volumes. In contrast to metallic $SrVO_3$, here we clearly see an extended plateau of $S_{imp}(T) = \log(6)k_B$ around 1000 K, which signals complete degeneracy of the t_{2g} shell, and its slight decrease at 300 K in proximity to the AFM state.

The isostructural transitions of cerium attracted a lot of experimental and theoretical effort, but its theoretical understanding is still controversial. On the basis of the DFT + DMFT calculation McMahan et al. [19] proposed that the total energy exhibits a double-minimum shape, concomitant with the appearance of the quasiparticle peak
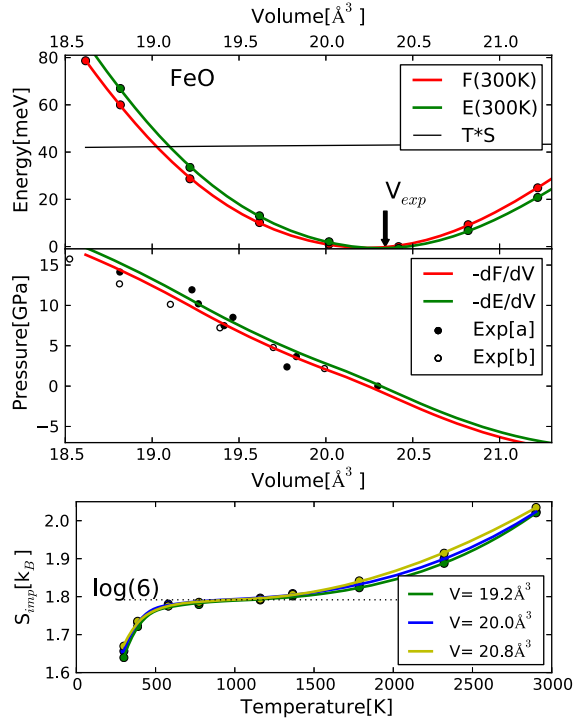
FIG. 2 (color online).   (a) $E(V)$ and $F(V)$ for FeO from Eqs. (1) and (4), respectively. Entropy term $TS_{\mathrm{imp}}(V)$ is large but almost constant. (b) Theoretical and experimental $p(V)$. Filled and empty circles are from Refs. [52] and [53], respectively. (c) Impurity entropy Eq. (7) for representative volumes. The degeneracy of the t_{2g} shell above 1000 K is apparent.
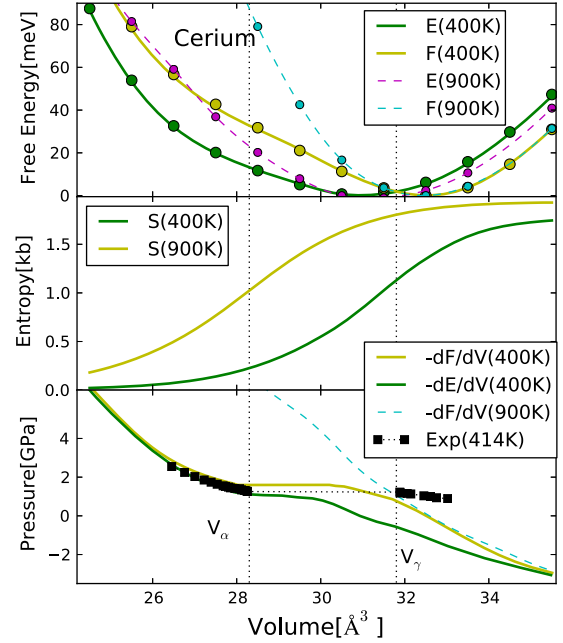

FIG. 3 (color online).   (a) $E(V)$ and $F(V)$ for elemental cerium from Eqs. (1) and (4), respectively. Data are presented for $T = 400$ and 900 K. (b) Entropy $S_{\mathrm{imp}}(V)$ is large and changes dramatically across the transition. (c) Theoretical and experimental [57] $p(V)$ diagram.

at a temperature as high as 1500 K, signaling the first order transition. Using a different implementation of the same method, Amadon *et al.* [35,54] proposed that the transition is entropy driven, and that the total energy is featureless with the minimum corresponding to the low volume α phase. Only the addition of the entropy term moves the minimum to the larger volume of the γ phase. In this picture the transition at low temperatures, where the entropy becomes small and cannot drive the transition, is intrinsically absent. Yet another proposal was recently put forward on the basis of LDA + Gutzwiller calculations [55,56], in which the transition is present even at zero temperature, but the transition occurs at negative pressure. The transition is thus detectable even in the total energy, in the absence of entropy, and becomes second order at $T = 0$. In the same method, the finite temperature transition is first order, and the double-minimum shape of free energy becomes most pronounced at a very high temperature (1500 K) [56].

Our DFT + DMFT results for Ce are plotted in Fig. 3. The total energy curve at 400 K clearly shows a region of very flat shape in the region between the α-γ volume. Indeed the derivative of the energy $-dE/dV$ displayed in Fig. 3(c) shows a clear region of zero slope around 1 GPa. This is consistent with results of Lanata *et al.* [55] finding a very similar zero slope of $-dE/dV$ at zero temperature, but

is inconsistent with Ref. [35], which finds no feature in the total energy. It is also inconsistent with McMahan *et al.* [19], showing a clear double-peak in the total energy. On the other hand, the addition of entropy substantially increases the region of soft volume, as suggested by Amadon *et al.* [54]. Indeed the change of the entropy between the two phases is of the order of $0.9k_B$, which is consistent with experimental estimations of 30 meV at 400 K [58]. The physical mechanism behind this large entropy change and unusual volume dependence of energy is in the very fast variation of coherence temperature, as suggested in Refs. [19,54], and conjectured in the Kondo volume collapse theory [59]. The phase transition in our calculation occurs around 1.6 GPa, which is not far from the experimentally determined critical pressure of 1.25 GPa at $T = 400$ K. The free energy barrier in our calculation is however extremely small, and no clear double peak of $F(V)$ or negative slope of $-dF/dV$ can be detected within our 1 meV precision of energies. This is similar to the results of Ref. [56] at 400 K, but different from Ref. [19]. While the start of the transition region in the α phase is in good agreement with experiment, the γ-phase volume is underestimated in our calculation. We believe that the addition of phonon entropy is needed to further increase the transition region, and establish a larger free energy barrier between the two phases. Experimentally, above 460 K the α-γ phase transition ends with the finite temperature critical point. Our calculation at the high temperature of 900 K shows that the signature of the phase transition in $F(V)$ and

$E(V)$ disappears, which is different than predicted by the Gutzwiller method [56], where the largest free energy barrier is found at these elevated temperatures, but qualitatively consistent with Ref. [19].

In summary, we successfully implemented the stationary formula for the free energy of the DFT + DMFT method. On the example of $SrVO_3$, FeO, and Ce metal, we demonstrated that the method successfully predicts lattice volumes in correlated solids, which are difficult for standard DFT functionals. We also resolved controversy in the mechanism of the α-γ transition in cerium.

[1] P. Hohenberg and W. Kohn, Phys. Rev. **136**, B864 (1964).
[2] A. E. Mattsson, R. Armiento, J. Paier, G. Kresse, J. M. Wills, and T. R. Mattsson, J. Chem. Phys. **128**, 084714 (2008).
[3] S. Y. Savrasov, G. Kotliar, and E. Abrahams, Nature (London) **410**, 793 (2001).
[4] See Supplemental Material at http://link.aps.org/supplemental/10.1103/PhysRevLett.115.256402 for technical details of the calculations, comparison of the results with standard functionals, and comments on the mass renormalization in $SrVO_3$, which includes Refs. [5–12].
[5] K. Ohta, R. E. Cohen, K. Hirose, K. Haule, K. Shimizu, and Y. Ohishi, Phys. Rev. Lett. **108**, 026403 (2012).
[6] A. McMahan, C. Huscroft, R. Scalettar, and E. Pollock, J. Comput.-Aided Mater. Des. **5**, 131 (1998).
[7] M. Weinert, E. Wimmer, and A. J. Freeman, Phys. Rev. B **26**, 4571 (1982).
[8] E. Gull, A. J. Millis, A. I. Lichtenstein, A. N. Rubtsov, M. Troyer, and P. Werner, Rev. Mod. Phys. **83**, 349 (2011).
[9] S. Skornyakov, A. Poteryaev, and V. Anisimov, Phys. Solid State **57**, 1431 (2015).
[10] J. P. Perdew, K. Burke, and M. Ernzerhof, Phys. Rev. Lett. **77**, 3865 (1996).
[11] J. P. Perdew, A. Ruzsinszky, G. I. Csonka, O. A. Vydrov, G. E. Scuseria, L. A. Constantin, X. Zhou, and K. Burke, Phys. Rev. Lett. **100**, 136406 (2008).
[12] M. Takizawa et al., Phys. Rev. B **80**, 235104 (2009).
[13] A. Georges and G. Kotliar, Phys. Rev. B **45**, 6479 (1992).
[14] A. Georges, G. Kotliar, W. Krauth, and M. J. Rozenberg, Rev. Mod. Phys. **68**, 13 (1996).
[15] V. I. Anisimov, A. I. Poteryaev, M. A. Korotin, A. O. Anokhin, and G. Kotliar, J. Phys. Condens. Matter **9**, 7359 (1997).
[16] A. I. Lichtenstein and M. I. Katsnelson, Phys. Rev. B **57**, 6884 (1998).
[17] G. Kotliar, S. Y. Savrasov, K. Haule, V. S. Oudovenko, O. Parcollet, and C. A. Marianetti, Rev. Mod. Phys. **78**, 865 (2006).
[18] S. Y. Savrasov, G. Kotliar, and E. Abrahams, Nature (London) **410**, 793 (2001).
[19] K. Held, A. K. McMahan, and R. T. Scalettar, Phys. Rev. Lett. **87**, 276404 (2001).
[20] A. K. McMahan, K. Held, and R. T. Scalettar, Phys. Rev. B **67**, 075108 (2003).
[21] B. Amadon, S. Biermann, A. Georges, and F. Aryasetiawan, Phys. Rev. Lett. **96**, 066402 (2006).
[22] S. Y. Savrasov, K. Haule, and G. Kotliar, Phys. Rev. Lett. **96**, 036404 (2006).
[23] L. V. Pourovskii, B. Amadon, S. Biermann, and A. Georges, Phys. Rev. B **76**, 235101 (2007).
[24] I. Leonov, N. Binggeli, D. Korotin, V. I. Anisimov, N. Stojić, and D. Vollhardt, Phys. Rev. Lett. **101**, 096405 (2008).
[25] I. Di Marco, J. Minár, S. Chadov, M. I. Katsnelson, H. Ebert, and A. I. Lichtenstein, Phys. Rev. B **79**, 115111 (2009).
[26] M. Aichhorn, L. Pourovskii, and A. Georges, Phys. Rev. B **84**, 054529 (2011).
[27] G. Lee et al., Phys. Rev. Lett. **109**, 177001 (2012).
[28] B. Amadon, J. Phys. Condens. Matter **24**, 075604 (2012).
[29] I. Leonov, A. I. Poteryaev, V. I. Anisimov, and D. Vollhardt, Phys. Rev. B **85**, 020401 (2012).
[30] M. S. Litsarev, I. Di Marco, P. Thunström, and O. Eriksson, Phys. Rev. B **86**, 115116 (2012).
[31] O. Grns, I. D. Marco, P. Thunstrm, L. Nordstrm, O. Eriksson, T. Bjrkman, and J. Wills, Comput. Mater. Sci. **55**, 295 (2012).
[32] D. Grieger, C. Piefke, O. E. Peil, and F. Lechermann, Phys. Rev. B **86**, 155121 (2012).
[33] L. V. Pourovskii, T. Miyake, S. I. Simak, A. V. Ruban, L. Dubrovinsky, and I. A. Abrikosov, Phys. Rev. B **87**, 115130 (2013).
[34] I. Leonov, V. I. Anisimov, and D. Vollhardt, Phys. Rev. Lett. **112**, 146401 (2014).
[35] J. Bieder and B. Amadon, Phys. Rev. B **89**, 195132 (2014).
[36] S. Mandal, R. E. Cohen, and K. Haule, Phys. Rev. B **89**, 220502 (2014).
[37] H. Park, A. J. Millis, and C. A. Marianetti, Phys. Rev. B **89**, 245133 (2014).
[38] H. Park, A. J. Millis, and C. A. Marianetti, Phys. Rev. B **90**, 235103 (2014).
[39] K. Haule, C.-H. Yee, and K. Kim, Phys. Rev. B **81**, 195107 (2010).
[40] Note that Pulay forces appear when the incomplete basis set is used.
[41] G. Baym, Phys. Rev. **127**, 1391 (1962).
[42] J. M. Luttinger and J. C. Ward, Phys. Rev. **118**, 1417 (1960).
[43] G. Baym and L. P. Kadanoff, Phys. Rev. **124**, 287 (1961).
[44] K. Haule, Phys. Rev. B **75**, 155113 (2007).
[45] P. Werner, A. Comanac, L. de' Medici, M. Troyer, and A. J. Millis, Phys. Rev. Lett. **97**, 076405 (2006).
[46] K. Held, A. K. McMahan, and R. T. Scalettar, Phys. Rev. Lett. **87**, 276404 (2001).
[47] P. Blaha, K. Schwarz, G. K. H. Madsen, D. Kvasnicka, and J. Luitz, WIEN2K, An Augmented Plane Wave+Local Orbitals Program for Calculating Crystal Properties (Karlheinz Schwarz, Techn. Universität Wien, Austria, 2001).

[48] K. Haule, T. Birol, and G. Kotliar, Phys. Rev. B **90**, 075136 (2014).

[49] K. Haule, Phys. Rev. Lett. **115**, 196403 (2015).

[50] R. Hrubiak, Ph.D. thesis, Florida International University, 2012, http://digitalcommons.fiu.edu/cgi/viewcontent.cgi?article=1802&context=etd.

[51] J. B. Goodenough and M. Longo, SpringerMaterials, The Landolt-Börnstein Database, **4a** (1970), http://dx.doi.org/10.1007/10201420_50.

[52] T. Yagi, T. Suzuki, and S.-I. Akimoto, J. Geophys. Res.: Solid Earth **90**, 8784 (1985).

[53] R. L. Clendenen and H. G. Drickamer, J. Chem. Phys. **44**, 4223 (1966).

[54] B. Amadon, S. Biermann, A. Georges, and F. Aryasetiawan, Phys. Rev. Lett. **96**, 066402 (2006).

[55] N. Lanatà, Y.-X. Yao, C.-Z. Wang, K.-M. Ho, J. Schmalian, K. Haule, and G. Kotliar, Phys. Rev. Lett. **111**, 196801 (2013).

[56] N. Lanatà, Y.-X. Yao, C.-Z. Wang, K.-M. Ho, and G. Kotliar, Phys. Rev. B **90**, 161104 (2014).

[57] M. J. Lipp, D. Jackson, H. Cynn, C. Aracne, W. J. Evans, and A. K. McMahan, Phys. Rev. Lett. **101**, 165703 (2008).

[58] F. Decremps, L. Belhadi, D. L. Farber, K. T. Moore, F. Occelli, M. Gauthier, A. Polian, D. Antonangeli, C. M. Aracne-Ruddle, and B. Amadon, Phys. Rev. Lett. **106**, 065701 (2011).

[59] J. W. Allen and L. Z. Liu, Phys. Rev. B **46**, 5047 (1992).